Geometry of optimal path hierarchies

Laurent Talon[1], Harold Auradou[1], Marc Pessel[2,3] and Alex Hansen[4]

[1] *Université de Paris-Sud, CNRS, FAST - Bât. 502, Campus Univ., Orsay, F-91405, France, EU*
[2] *Université de Paris-Sud, IDES, UMR8148 - F-91405 Orsay, France, EU*
[3] *CNRS - F-92405 Orsay, France, EU*
[4] *Department of Physics, Norwegian University of Science and Technology - N-7491 Trondheim, Norway*

Abstract – We investigate the hierarchy of optimal paths in a disordered landscape, based on the best path, the second best path and so on in terms of an energy. By plotting each path at a height according to its energy above some zero level, a landscape appears. This landscape is self-affine and controlled by two Hurst exponents: the one controlling the height fluctuations is $1/3$ and the one controlling the fluctuations of the equipotential lines in the landscape is $2/3$. These two exponents correspond to the exponents controlling energy and shape fluctuations in the directed polymer problem. We furthermore find that the density of spanning optimal paths scale as the length of the paths to $-2/3$ and the histogram of energy differences between consecutive paths scale as a power law in the difference size with exponent -2.5.

Introduction. – The optimal path between two points in a disordered landscape lies at the heart of a large number of problems in physics and technology. Internet routing [1], sensor networks [2], or more generally complex networks [3–5], are important areas where optimal paths are essential even though the "landscape" in this case is a complex network. Surface growth phenomena [6] that are describable by the Kardar-Parisi-Zhang equation [7], but also the simpler Eden growth phenomenon, may be related to the optimal path problem [8]. In both cases, the optimal path problems appears in a form equivalent to the *directed polymer problem* [9,10]. This problem consists in exploring the configurations of a polymer that binds locally to a static but disordered substrate in such a way that it contains no back bends. At zero temperature, this is an optimal path problem. It has been known for a long time that the statistics of such polymers —or optimal paths— reflects an underlying ultrametric structure [11,12]. The directed polymer problem shows up in a number of different physical problems such as in plasticity [13], in tracer transport in porous media [14] and in non-Newtonian fluid flow in porous media [15,16].

We consider a two-dimensional landscape. To each point $\vec{r} = (x, y)$ in this landscape, we assign a positive number —an "energy"— $t(\vec{r})$. For the time being,

we assume that $t(\vec{r})$ is a spatially uncorrelated noise. We imagine a path $\mathcal{P}$ through this landscape $\vec{r}(l) \in \mathcal{P}$, parametrized by its length l from the starting point, such that $\vec{r}(0) = \vec{r}_i$ and $\vec{r}(L) = \vec{r}_f$, where $\vec{r}_i$ and $\vec{r}_f$ are the start and end points of the path, respectively. We then define the *optimal path* between $\vec{r}_i$ and $\vec{r}_f$ as

$$T_1 = \min_{\vec{r} \in \mathcal{P}} \int_0^L t(\vec{r}(l)) \, \mathrm{d}l, \qquad (1)$$

where the minimization is taken over all possible paths. The value T_1 is the "energy" of the optimal path. The optimal path will contain no loops and if the disorder is not too strong, it will have no back bends: it will be directed [17]. If we average over an ensemble of landscapes, we find that the fluctuations in T, $\Delta T = \langle (T - \langle T \rangle)^2 \rangle^{1/2}$ scale as

$$\Delta T \sim L^\omega, \qquad (2)$$

and the fluctuations of the optimal path Δx when the two end points $\vec{r}_i$ and $\vec{r}_f$ have been placed along the y-axis a distance L apart,

$$\Delta x \sim L^\nu. \qquad (3)$$

We have that $\omega = 1/3$ and $\nu = 2/3$ [9,10]. These two exponents are manifestations of the ultrametricity of the optimal paths.
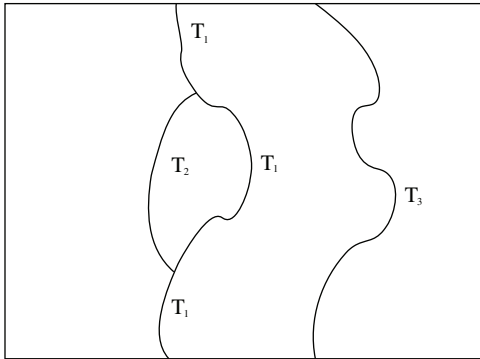
Fig. 1: Three optimal paths —the best, the second best and the third best— are shown. They are characterized by the energies T_1, T_2 and T_3 with the ordering $T_1 < T_2 < T_3$.

Fig. 2: (Color online) A complete pathscape showing the optimal path passing through each link in the 1024×512 size lattice by a color code: darker color corresponds to lower value of T and lighter color to higher value.

Recently, there has been an interest in going beyond the optimal path and ask about the second best path, third best path and so on. This was investigated by Andrade *et al.* [18]. They identified a hierarchy of optimal paths by the following algorithm: identify the largest t-value along the optimal path. Change the value of this t to such a large value that the optimal path is no longer optimal. A new path will become optimal. Repeat this. This will produce a hierarchy of optimal paths which has very interesting scaling properties. However, this hierarchy is intimately connected with the maximum value along the optimal path and the hierarchy that is produced reflects the procedure.

The pathscape. – In this letter we will consider a different hierarchy of optimal paths. Without changing any values of t, we identify the path that has the smallest value of T, defined in eq. (1), the path that has the second smallest value of T associated with it etc. We number the paths $T_1 < T_2 < T_3 < \cdots$. We identify the optimal path by considering every point $\vec{r}$ in the landscape and identify the optimal path with the prescribed start and end point which passes through $\vec{r}$. We may then associate the corresponding T value to each point $\vec{r}$, where T is the value of the energy of the optimal path passing through that point. We show in fig. 1 an example of how the three first paths of such a hierarchy may look. Each path starts at the lower edge and ends at the upper edge of the landscape. In the example, there is overlap between the T_1 and T_2 paths whereas T_3 is independent.

In fig. 2 we have identified the optimal paths through each node in a square lattice starting at the lower edge and ending at the upper edge. Each node is color coded according to the value of the energy T of the optimal path passing through it: darker color means lower value of T whereas lighter color means higher value of T. We will refer to this landscape of paths as a *pathscape*. In the following we describe the algorithm that produced it.

The distribution of t we consider in the following is $p(t) = t^{-2}$ where $t > 1$. There are no spatial correlations. This is the natural yield threshold distribution found, *e.g.*,
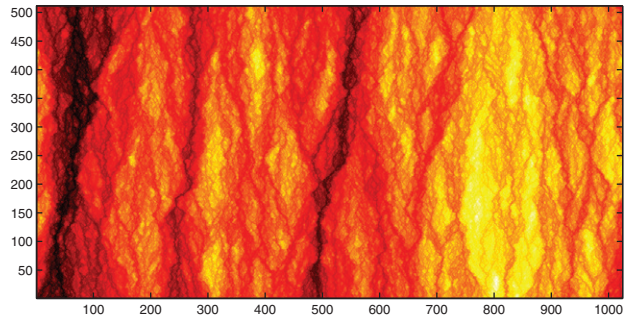
in connection with flow of non-Newtonian fluids in porous media, see [16].

Identifying the pathscape. We generalize the iterative algorithm proposed in ref. [17] to identify optimal paths on a lattice. Each link $\vec{r}_{i,j}$ linking neighboring nodes $\vec{r}_i$ and $\vec{r}_j$ for all i and j is assigned a threshold $t_{i,j}$. We assign to each node $\vec{r}_i$ a variable V_i. Initially, we set this variable to zero for all nodes to be updated. These are the nodes that constitute the interior of the region of interest. On the boundary of the region, the nodes are not updated. The updating proceeds as follows. If $j(i)$ are the addresses of the links adjacent to node $\vec{r}_i$, we update the node

$$V_i \rightarrow V_i = \min_{j(i)} \left(t_{i,j(i)} + V_{j(i)} \right). \tag{4}$$

After N updates, the value V_i will contain the sum of the tresholds along the optimal path originating in $\vec{r}_i$ of length N. There are no restrictions on the shape of this optimal path. It may well curl up on itself, thus forming a "tadpole" configuration.

We now consider the boundary of the region in which the optimal paths are situated. The nodes that form the edges of the network constitute the boundary. We now single out one node, $\vec{r}_0$, on the boundary and demand that we identify the optimal paths starting from any internal node and ending at this particular boundary node. To do this, we set the value $V_{\vec{r}_0} = 0$ and the value of all other boundary nodes to a very large value M. We then iterate the internal nodes according to (4) until the value of V_i for all internal nodes no longer changes. Then V_i contains the sum $T_{i,0}$, defined in eq. (1), between internal node $\vec{r}_i$ and boundary node $\vec{r}_0$. Let us now choose another internal node $\vec{r}_j$, which is neighbor to the previously considered internal node $\vec{r}_i$, and boundary node $\vec{r}_1$. We repeat the recipe above, and identify the optimal path starting at any internal node $\vec{r}_j$ and ending at the boundary at $\vec{r}_1$, $T_{j,1}$. We also calculate $T_{i,1}$ and $T_{j,0}$. This allows us to calculate the energy of the optimal path that starts at boundary node $\vec{r}_0$, ends at boundary node $\vec{r}_1$ and *passes*
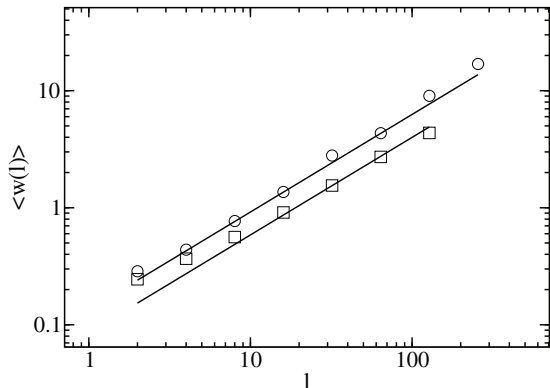
Fig. 3: Averaged wavelet coefficients $\langle w(l) \rangle$ measured orthogonal to the flow direction ($\circ$) and parallel to the flow direction ($\square$) as a function of the length scale l. The straight lines both have slopes equal to 5/6, making the surfaces self-affine with the Hurst exponent $H = 1/3$ in both directions. The figure is based on one sample of size 1024×512.

by node $\vec{r}_i$ by the expression

$$T_{0,i,1} = \min_{j(i)} \left(T_{0,i} + t_{i,j(i)} + T_{j(i),1}, T_{0,j(i)} + t_{j(i),i} + T_{i,1} \right).$$
(5)

which is the optimal path starting at $\vec{r}_0$, ending at $\vec{r}_1$ and passing by $\vec{r}_i$.

We now set the V-value associated with each node on the lower edge on the lattice to zero while setting the V-value associated with each node on the upper edge to M. By iterating the algorithm as described above will then determine the energy of the optimal path starting at any internal node i and ending somewhere on the lower edge. By repeating this calculation but with the V-values switched between the upper and lower edges, we find the optimal paths starting at any internal node and ending at the upper edge. These two sets of energies may now be combined as prescribed in eq. (5) to identify the hierarchy of all optimal paths starting at the lower edge and ending at the upper edge. By assigning to each optimal path its energy and plotting them at the corresponding height above the zero level, an optimal *pathscape* appears. This is shown in fig. 2, which is based on a square lattice where the lower edge forms the set $\{\vec{r}_0\}$ and the upper boundary forms the set $\{\vec{r}_1\}$. The two other edges are identified with each other, making the system periodic in this direction. The threshold values $t_{\vec{R}}$ were chosen from a flat distribution on the unit interval. The distance between the lower and upper edges of the lattice is $L = 1024$ and the width of the lattice is $W = 512$.

The "pathscape" of fig. 2 contains the hierarchy of optimal paths in this system. There is a minimum path which is the optimal path between the upper and lower edges. But, there is also the second best path, the third best path etc. as illustrated in fig. 1.

Geometry of the pathscape. The hierarchy of optimal paths, shown as a "pathscape" in fig. 2, has many
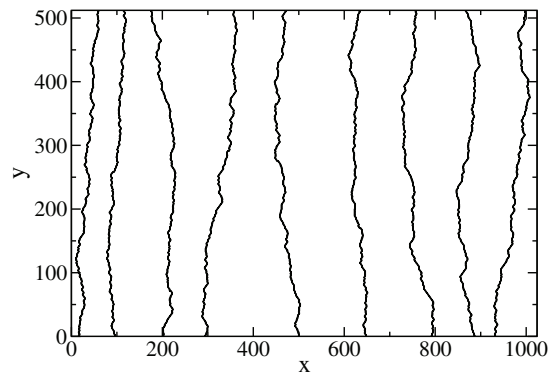
Fig. 4: The spanning paths in a 1024×512 system.
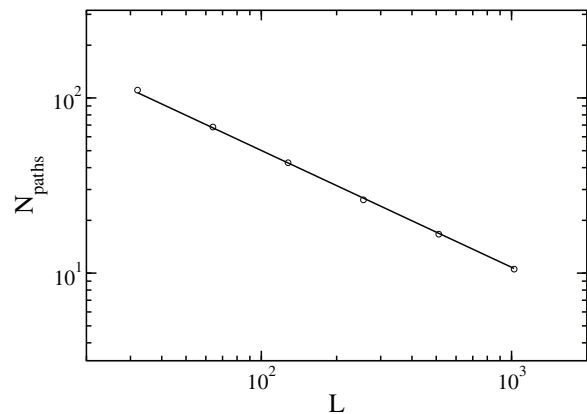
Fig. 5: Number of spanning paths N_{path} as a function of system length L, while keeping W fixed and equal to 2048. The number of samples were as follows: $L = 32$: 2000, $L = 64$: 1000, $L = 128$: 500, $L = 256$: 250, $L = 512$: 125 and $L = 1024$: 63. The straight line corresponds to the power law $N_{\mathrm{path}} \sim L^{-2/3}$.

interesting properties. Given the "pathscape" of optimal paths, the two exponents ω and ν defined in eqs. (2) and (3) may be given a geometrical interpretation. In fig. 3, we have made cuts through the pathscape in the x- and in the y-direction, measuring T along it. We have then wavelet transformed the functions using the DAUB-4 wavelet basis [19] and averaged over the absolute value of the ensuing wavelet coefficients. The figure shows the average wavelets as a function of the scale l. If the signal that has been wavelet transformed is self-affine with the Hurst exponent H, the wavelet coefficients $\langle W(l) \rangle \sim l^{H+1/2}$ [20]. We find that $H + 1/2 = 5/6$ fits the data excellently both for the curves along the x- and the y-directions. This makes $H = 1/3$. It is then very natural to interpret the exponent ω, defined in eq. (2), as being the Hurst exponent of the pathscape, $\omega = H = 1/3$. The second exponent, $\nu = 2/3$, is the Hurst exponent of equipotential curves in the "pathscape"[1].

---

[1]Hence, the "slit island" relation of Mandelbrot [21,22] that relates the Hurst exponent H of a landscape to the fractal dimension of the equipotential curves d_f does not work here as it would predict
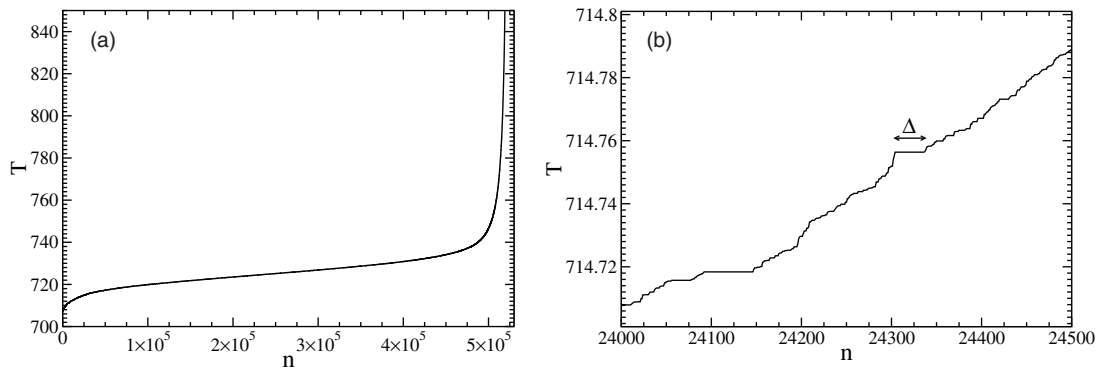
Fig. 6: (a) The ordered sequence of optimal path energies T. A given point along this curve shows the number of links that have T or less as threshold. (b) A detail of (a). The steps are clearly visible and their size Δ is defined. The data are based on one sample of size 512×512.
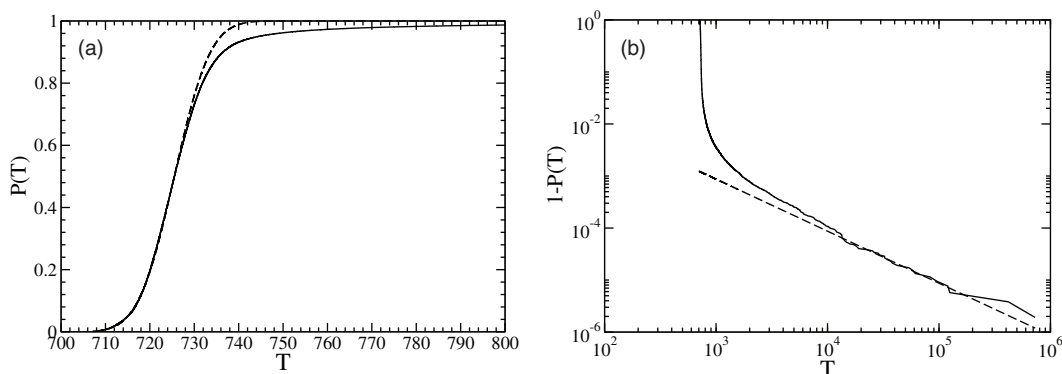
Fig. 7: (a) The cumulative probability $P(T)$ of the energies of the optimal paths of fig. 6. The broken curve shows $[1 + \mathrm{erf}(0.111[T - 725.5])]/2$. (b) $1 - P(T)$ *vs.* T. The broken straight line is $0.87T^{-1}$. Such an asymptotic law is expected from the distribution of the t values that we have used.

We now single out the *spanning paths* in the "path-scape" which are those opimal paths that form local minima in T, see fig. 4. In fig. 1, the paths labeled T_1 and T_3 are spanning paths, the one labeled T_2 is not. Since the Hurst exponent of these paths is $\nu = 2/3$, their density, N_{paths} must scale as

$$N_{\mathrm{paths}} \sim L^{-\nu}. \qquad (6)$$

In fig. 5, we plot N_{paths} against L. Equation (6) is obeyed.

We now consider the distribution of energies T in the "pathscape." We show the ordered sequence of T-values in fig. 6(a). That is, a given point along this curve shows the number of links n that have a value T or less associated with them. The particular shape of this curve reflects the distribution of t-values used and is not universal. In fig. 7(a), we have replotted and rescaled these data so that they now are represented as a cumulative probability; $P(T)$ is the probability to find a path with energy less than or equal to T. On top of this curve, we have plotted the function $[1 + \mathrm{erf}(0.111[T - 725.5])]/2$. This shows that the probability distribution of energies is Gaussian

---

$d_f = 4/3$. The equipotential curves have $d_f = 1$. The reason for this is the anisotropy of the "pathscape."
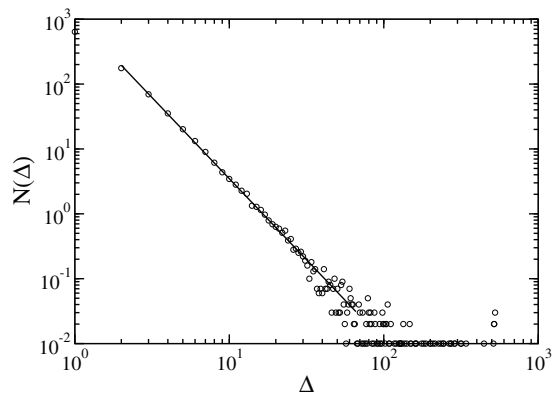
Fig. 8: Histogram $N(\Delta)$ over the number of links Δ that simultaneously hit their optimal path thresholds. The straight line has a slope equal to -2.5. The figure is based on 100 samples of size 1024×512.

for values of T a little beyond the median. However, for large values of T the distribution changes character. In fig. 7(b), we show that $P(T) = 1 - 0.87\,T^{-1}$ fit the data well: the distribution of energies is Gaussian —as expected for self-affine surfaces— but with a fat tail. This fat tail

reflects the distribution of local energies, $p(t) = t^{-2}$ on the unit interval, that was used and is not a universal feature.

In fig. 6(b), we show a closeup of the curve. It consists of a series of horizontal steps. A step at value T shows how many links that belong to an optimal path with that given T-value. In fig. 8 we show a histogram of the steps. They follow the power law $N(\Delta) \sim \Delta^{-\tau}$. The value $\tau = 5/2$ fits the data very well. This is the value that is expected for an uncorrelated random walk process with a diminishing bias, see [23,24]. It is surprising to see the same value in this system which is highly correlated.

Conclusion. – We have studied in this letter the geometry of the pathscape formed by the hierarchy of optimal paths by identifying the optimal path passing through each point in the disordered landscape. The pathscape is a self-affine surface with a Hurst exponent $H = 1/3$ but with a strong anisotropy in the amplitudes. This allows us to interpret the two exponent ω and ν (eqs. (2) and (3)), controling the fluctuations of the energy and shape of the optimal paths, respectively, as the Hurst exponents describing the pathscape height fluctuations and equipotential line fluctuations, respectively. We have found that the density of optimal paths that span the system scales with the length of paths to minus the Hurst exponent, eq. (6). We have furthermore investigated the structure of the sequence of optimal paths in the hierarchy, finding that the histogram of distances between energies scales as the distance to the power minus 2.5.

We have chosen a wide distribution of t-values for our numerical study. As demonstrated by Hansen and Kertesz [17], the directed polymer universality class is very stable; it takes an extreme disorder to move away from this problem. As long as the optimal path, characterized by T_1 is in the directed polymer universality class, the pathscape will have the structure that we have presented here.

$$* * *$$

REFERENCES

[1] Valverde S. and Sole R. V., *Eur. J. Phys. B*, **38** (2004) 245.

[2] Shah R. C. and Rabaey J. M., *2002 IEEE Wireless and Networking Conference (WCNC 2002)*, Vol. **1** (IEEE) 2002, p. 350.

[3] Braunstein L. A., Buldyrev S. V., Cohen R., Havlin S. and Stanley H. E., *Phys. Rev. Lett.*, **91** (2003) 168701.

[4] Havlin S., Braunstein L. A., Buldyrev S. V., Cohen R., Kalisky T., Sreenivasan S. and Stanley H. E., *Physica A*, **246** (2005) 82.

[5] Yang R., Wang W. X., Lai Y. C. and Chen G., *Phys. Rev. E*, **79** (2009) 026112.

[6] Barabasi A. L. and Stanley H. E., *Fractal Concepts in Surface Growth* (Cambridge University Press, Cambridge) 1995.

[7] Kardar M., Parisi G. and Zhang Y. C., *Phys. Rev. Lett.*, **56** (1986) 889.

[8] Roux S., Hansen A. and Hinrichsen E. L., *J. Phys. A*, **24** (1991) L295.

[9] Huse D. A. and Henley C. L., *Phys. Rev. Lett.*, **54** (1985) 2708.

[10] Kardar M. and Zhang Y. C., *Phys. Rev. Lett.*, **58** (1987) 2087.

[11] Perlsman E. and Schwartz M., *Europhys. Lett.*, **17** (1992) 11.

[12] Rammal R. and Toulouse G., *Rev. Mod. Phys.*, **58** (1986) 765.

[13] Hansen A., Hinrichsen E. L. and Roux S., *Phys. Rev. Lett.*, **66** (1992) 2476.

[14] Devillard P., *Phys. Rev. Lett.*, **70** (1993) 1124.

[15] Roux S. and Herrmann H. J., *Europhys. Lett.*, **4** (1987) 1227.

[16] Chen M., Rossen W. and Yortsos Y. C., *Chem. Eng. Sci.*, **60** (2005) 4183.

[17] Hansen A. and Kertesz J., *Phys. Rev. Lett.*, **93** (2004) 040601.

[18] Andrade J. S. jr., Oliveira E. A., Moreira A. A. and Herrmann H. J., *Phys. Rev. Lett.*, **103** (2009) 225503.

[19] Press W. H., Teukolsky S. A., Vetterling W. T. and Flannery B. P., *Numerical Recipes*, 3rd edition (Cambridge University Press, Cambridge) 2007.

[20] Simonsen I., Hansen A. and Nes O. M., *Phys. Rev. E*, **58** (1998) 2779.

[21] Mandelbrot B. B., *Phys. Scr.*, **32** (1988) 257.

[22] Feder J., *Fractals* (Plenum, New York) 1988.

[23] Hemmer P. C. and Hansen A., *ASME J. Appl. Mech.*, **59** (1992) 909.

[24] Pradhan S., Hansen A. and Chakrabarti B. K., *Rev. Mod. Phys.*, **82** (2010) 499.